

Supporting Information

Real-Time Detection of Metal Ions with Conjugated Polymer Composite Papers

Ji Eun Lee,^{†,‡,§} Hyeon Woo Shim,^{†,‡,§} Oh Seok Kwon,[†] Yang-Il Huh,^{‡,§} and Hyeonseok Yoon^{†,‡,§,}*

[†]Alan G. MacDiarmid Energy Research Institute, [‡]Department of Polymer and Fiber System Engineering, Chonnam National University, 77 Yongbong-ro, Buk-gu, Gwangju 500-757, South Korea.

[§]Department of Polymer Engineering, Graduate School, Chonnam National University, 77 Yongbong-ro, Buk-gu, Gwangju 500-757, South Korea.

[†]Department of Chemical and Environmental Engineering, School of Engineering and Applied Science, Yale University, New Haven, Connecticut 06511, United States

* To whom correspondence should be addressed.

Email: hyoon@chonnam.ac.kr

1. Additional Experimental Details
2. FT-IR Spectroscopy Analysis
3. Mechanical Adhesion Test
4. Cyclic Voltammetry Analysis
5. Analytical Parameters of Response Profiles
6. Principal Component Analysis Plots
7. Reproducibility in Response
8. Kinetic Binding Parameters
9. Real Sample Test

1. Additional Experimental Details

Materials. Pyrrole (98%) and alpha-cellulose paper (>98%, 55 mm in diameter) were purchased from Sigma-Aldrich and Whatman, respectively. Ferric chloride ($\geq 98\%$) was obtained from Merck. Metal salts reagents were purchased from Sigma-Aldrich. Carbon paste and nickel plate were used as conductive binder and working electrode, respectively. Standard metal ion solutions were prepared by dissolving the appropriate amounts of nitrate salts (Ag(I), Pb(II), Ni(II), Cd(II), Cr(III), Zn(II)) or chloride salt (Hg(II)) in distilled water (pH 7).

Characterization. SEM was conducted using a JEOL JSM-7500F microscope to observe the morphology of the PPCL papers. The specimens were coated with a thin layer of gold to eliminate charging effects. Fourier transform infrared (FT-IR) spectra were obtained using a Shimadzu 8200 spectrometer. Adhesion tests were performed with a 180° peeling geometry at 30 mm min^{-1} using a Universal Testing Machine STM-5, in which a peeling 3M Scotch 600 adhesive tape was used, and the sample size was $25 \text{ mm} \times 60 \text{ mm}$. All electrochemical measurements were conducted using a Wonatech WMPG 1000 potentiostat/galvanostat.

2. FT-IR Spectroscopy Analysis

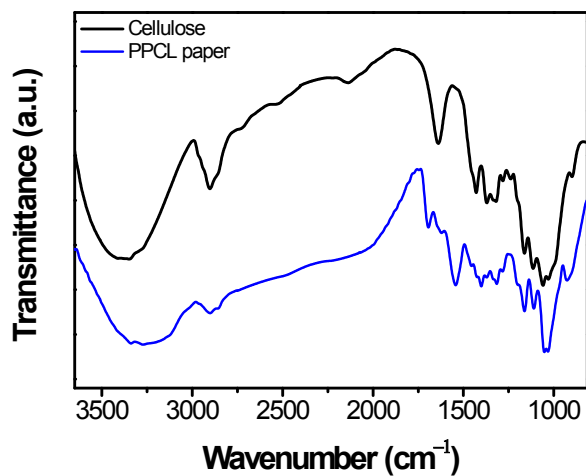


Figure S1. FT-IR spectra of PPCL papers and cellulose (control).

Figure S1 compares the FT-IR spectra of the PPCL paper and cellulose. On the spectrum of cellulose, the strong peaks at 3380, 2900, and 1640 cm^{-1} are attributed to O–H stretching, C–H stretching, and bound water within the cellulose structure, respectively. Additionally the peaks at 1370, 1320, and 1160 cm^{-1} correspond to C–H bending, C–H in-plane bending, and C–O–C asymmetric stretching. The characteristic peaks of polypyrrole at 3270 and 1690–1460 cm^{-1} , which are absent in those of cellulose, demonstrated the presence of polypyrrole on cellulose. The peaks at 3270 and 1690–1460 cm^{-1} arise from N–H stretching and conjugated pyrrole ring stretching.

3. Mechanical Adhesion Test

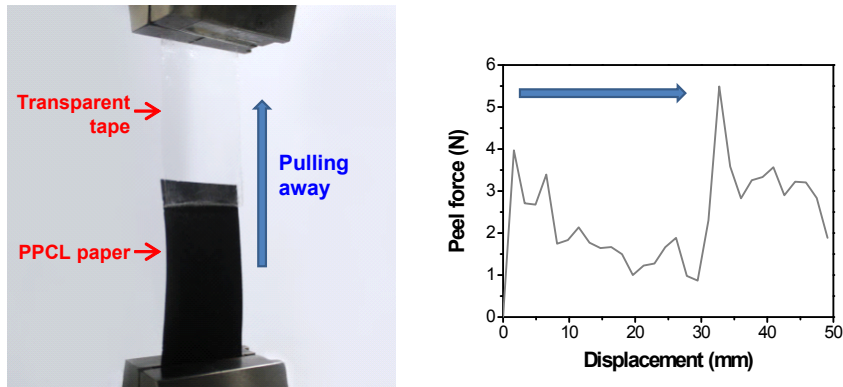


Figure S2. (a) Photograph describing the mechanical adhesion test: transparent adhesive tape is being pulled away from the PPCL paper. (b) Force-distance curve of the PPCL paper with the tape.

The PPCL paper was flexible and mechanically robust. The mechanical adhesion test for polypyrrole to cellulose in the composite paper was conducted with transparent adhesive tape. As shown in Figure S2a, the test was performed by peeling back the tape at 180 ° angle from the PPCL paper. No visible polypyrrole debris was observed on the detached tape, indicating that polypyrrole stuck well to the cellulose without peeling. The calculated average peel force was as high as 2.4 N during the test (Figure S2b). This result suggests that polypyrrole was strongly wrapped around the cellulose fibrils, which is essential for practical applications such as membranes and filters.

4. Cyclic Voltammetry Analysis

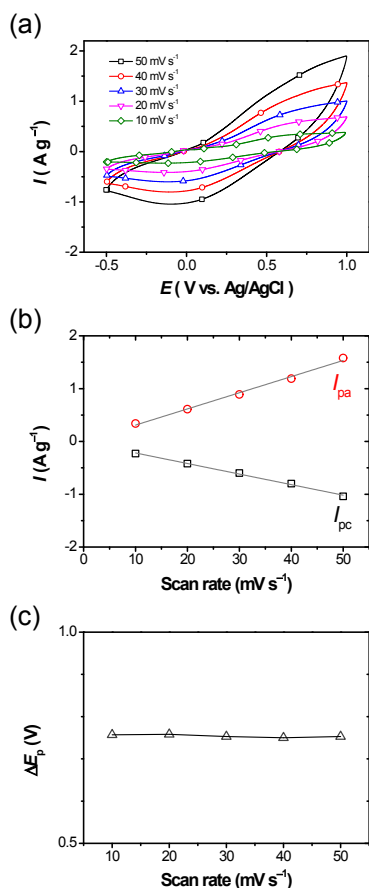


Figure S3. (a) Cyclic voltammograms of PPCL papers recorded at scan rates of 10 to 50 mV s^{-1} in 1 M H_2SO_4 solution. The current was normalized with respect to the mass of the sample. (b) Plots of the peak current (the anodic peak current, I_{pa} ; the cathodic peak current, I_{pc}) vs. the scan rate, and (c) plot of the peak potential separation vs. the scan rate.

Figure S3a displays the cyclic voltammograms of the PPCL paper measured at different scan rates from 10 to 50 mV. The electrochemical properties of the composite paper are determined by how the cellulose is coated with polypyrrole in terms of electrical and mechanical properties. The cyclic voltammograms all exhibited a similar shape, with a pair of broad redox peaks. The PPCL paper presents an oxidation peak at ca. 0.8 V and a reduction peak at ca. -0.2 V (vs. Ag/AgCl). The redox reaction of the PPCL paper

involves the transport of ions in and out of the polypyrrole to compensate the cationic nature of the oxidized, conductive polypyrrole. The resistance of the PPCL paper increases when polypyrrole is reduced under cathodic potentials and returns to its initial value upon subsequent oxidation. The increase in resistance is due to the change of polypyrrole from oxidized form to reduced form, and this process includes anion expulsion and/or cation incorporation. In the above scan rate range, the peak currents in the cyclic voltammograms are directly proportional to the scan rate, indicating that the redox process was surface controlled and that the electron transfer rate was rapid (Figure S3b). The peak to peak separations between the oxidation and reduction peaks were almost constant with a negligible deviation of 0.4 % (Figure S3c).

5. Analytical Parameters of Response Profiles

Table S1. Analytical parameters of the responses of PPCL papers to metal ions in the closed cell.

Metal ions	Potential (V)	Transition conc. (from linear to nonlinear) (M)	Detection limit (M)	Response magnitude (μA)	Response time (s)
Hg(II)	+1.0	$\sim 5 \times 10^{-6}$	1×10^{-6}	1.30 ± 0.08	≤ 5
	+0.5	$\sim 1 \times 10^{-4}$	1×10^{-5}	0.52 ± 0.04	
	0.0	$\sim 1 \times 10^{-4}$	1×10^{-5}	-4.40 ± 0.12	
	-0.5	$\sim 1 \times 10^{-4}$	1×10^{-5}	-0.53 ± 0.06	
	-1.0	$\sim 5 \times 10^{-6}$	1×10^{-6}	-5.81 ± 0.24	
Ag(I)	+1.0	$\sim 1 \times 10^{-5}$	5×10^{-6}	3.69 ± 0.18	≤ 5
	+0.5	$\sim 1 \times 10^{-4}$	5×10^{-5}	2.70 ± 0.09	
	0.0	$\sim 1 \times 10^{-4}$	5×10^{-5}	-18.65 ± 1.45	
	-0.5	$\sim 5 \times 10^{-5}$	5×10^{-5}	-28.51 ± 1.92	
	-1.0	$\sim 5 \times 10^{-5}$	1×10^{-5}	-6.53 ± 0.34	
Pb(II)	+1.0	$\sim 1 \times 10^{-4}$	5×10^{-6}	$2.23 \pm$	≤ 5
	+0.5	$\sim 1 \times 10^{-4}$	5×10^{-6}	$0.74 \pm$	
	0.0	$\sim 1 \times 10^{-4}$	5×10^{-6}	$-0.55 \pm$	
	-0.5	$\sim 1 \times 10^{-4}$	5×10^{-6}	$-1.12 \pm$	
	-1.0	$\sim 1 \times 10^{-4}$	1×10^{-7}	$-1.80 \pm$	
Ni(II)	+1.0	$\sim 1 \times 10^{-4}$	1×10^{-5}	3.32 ± 0.34	≤ 5
	+0.5	$\sim 1 \times 10^{-4}$	1×10^{-5}	1.81 ± 0.22	
	0.0	$\sim 1 \times 10^{-4}$	1×10^{-6}	-0.30 ± 0.03	
	-0.5	$\sim 1 \times 10^{-4}$	1×10^{-5}	-3.20 ± 0.28	
	-1.0	$\sim 1 \times 10^{-4}$	1×10^{-6}	-0.87 ± 0.04	
Cd(II)	+1.0	$\sim 1 \times 10^{-5}$	5×10^{-6}	3.35 ± 0.45	≤ 5
	+0.5	$\sim 1 \times 10^{-4}$	5×10^{-6}	0.95 ± 0.05	
	0.0	$\sim 1 \times 10^{-4}$	5×10^{-6}	-1.01 ± 0.19	
	-0.5	$\sim 1 \times 10^{-4}$	5×10^{-6}	-4.18 ± 0.54	
	-1.0	$\sim 1 \times 10^{-4}$	5×10^{-6}	-6.05 ± 0.43	
Cr(III)	+1.0	$\sim 1 \times 10^{-5}$	1×10^{-6}	1.52 ± 0.12	≤ 5
	+0.5	$\sim 1 \times 10^{-4}$	1×10^{-6}	0.39 ± 0.03	
	0.0	$\sim 5 \times 10^{-5}$	1×10^{-6}	-0.40 ± 0.05	
	-0.5	$\sim 1 \times 10^{-4}$	1×10^{-6}	-0.77 ± 0.08	
	-1.0	$\sim 1 \times 10^{-4}$	1×10^{-6}	-2.27 ± 0.20	
Zn(II)	+1.0	$\sim 1 \times 10^{-4}$	5×10^{-6}	2.51 ± 0.22	≤ 5
	+0.5	$\sim 1 \times 10^{-4}$	5×10^{-6}	0.70 ± 0.04	
	0.0	$\sim 1 \times 10^{-4}$	5×10^{-6}	-0.35 ± 0.09	
	-0.5	$\sim 1 \times 10^{-4}$	5×10^{-6}	-2.05 ± 0.35	
	-1.0	$\sim 1 \times 10^{-4}$	5×10^{-6}	-3.27 ± 0.69	

Table S2. Analytical parameters of the responses of PPCL papers to metal ions in the flow cell.

Metal ions	Potential (V)	Transition conc. (from linear to nonlinear) (M)	Detection limit (M)	Response magnitude (μ A)	Response time (s)
Hg(II)	+1.0	$\sim 1 \times 10^{-5}$	1×10^{-6}	4.88 ± 0.68	
	+0.5	$\sim 1 \times 10^{-4}$	1×10^{-5}	0.07 ± 0.01	
	0.0	$\sim 5 \times 10^{-5}$	1×10^{-6}	-0.32 ± 0.07	
	-0.5	$\sim 1 \times 10^{-5}$	5×10^{-6}	-0.94 ± 0.15	
	-1.0	$\sim 1 \times 10^{-5}$	5×10^{-6}	-2.26 ± 0.55	
Ag(I)	+1.0	$\sim 1 \times 10^{-5}$	5×10^{-6}	0.53 ± 0.10	
	+0.5	$\sim 1 \times 10^{-4}$	1×10^{-5}	0.47 ± 0.06	
	0.0	$\sim 1 \times 10^{-4}$	1×10^{-4}	-1.36 ± 0.11	
	-0.5	$\sim 1 \times 10^{-4}$	1×10^{-4}	-22.53 ± 5.34	
	-1.0	$\sim 5 \times 10^{-5}$	1×10^{-5}	-6.32 ± 1.88	
Pb(II)	+1.0	$\sim 1 \times 10^{-5}$	5×10^{-6}	1.20 ± 0.09	
	+0.5	$\sim 1 \times 10^{-4}$	5×10^{-5}	0.29 ± 0.04	
	0.0				
	-0.5	$\sim 5 \times 10^{-5}$	5×10^{-6}	-0.65 ± 0.09	
	-1.0	$\sim 5 \times 10^{-5}$	5×10^{-6}	-2.69 ± 0.27	
Ni(II)	+1.0	$\sim 1 \times 10^{-5}$	5×10^{-6}	1.59 ± 0.20	
	+0.5	$\sim 1 \times 10^{-4}$	5×10^{-6}	0.10 ± 0.03	
	0.0				≤ 10
	-0.5	$\sim 5 \times 10^{-5}$	5×10^{-5}	-9.50 ± 0.97	
	-1.0	$\sim 1 \times 10^{-5}$	5×10^{-6}	-2.04 ± 0.42	
Cd(II)	+1.0	$\sim 1 \times 10^{-4}$	5×10^{-6}	0.76 ± 0.11	
	+0.5	$\sim 5 \times 10^{-5}$	5×10^{-6}	0.24 ± 0.04	
	0.0	$\sim 1 \times 10^{-4}$	1×10^{-5}	-0.12 ± 0.03	
	-0.5	$\sim 1 \times 10^{-5}$	5×10^{-6}	-0.82 ± 0.09	
	-1.0	$\sim 1 \times 10^{-5}$	5×10^{-6}	-0.56 ± 0.13	
Cr(III)	+1.0	$\sim 5 \times 10^{-6}$	1×10^{-6}	2.77 ± 0.46	
	+0.5	$\sim 1 \times 10^{-4}$	1×10^{-5}	1.76 ± 0.39	
	0.0	$\sim 1 \times 10^{-4}$	5×10^{-5}	-0.26 ± 0.05	
	-0.5	$\sim 1 \times 10^{-5}$	5×10^{-6}	-2.53 ± 0.31	
	-1.0	$\sim 5 \times 10^{-6}$	1×10^{-6}	-9.25 ± 1.92	
Zn(II)	+1.0	$\sim 5 \times 10^{-5}$	1×10^{-5}	1.96 ± 0.33	
	+0.5	$\sim 1 \times 10^{-4}$	5×10^{-6}	0.16 ± 0.04	
	0.0	$\sim 1 \times 10^{-4}$	1×10^{-5}	-0.19 ± 0.04	
	-0.5	$\sim 5 \times 10^{-5}$	5×10^{-6}	-1.64 ± 0.21	
	-1.0	$\sim 1 \times 10^{-5}$	1×10^{-5}	-1.86 ± 0.25	

6. Principal Component Analysis Plots

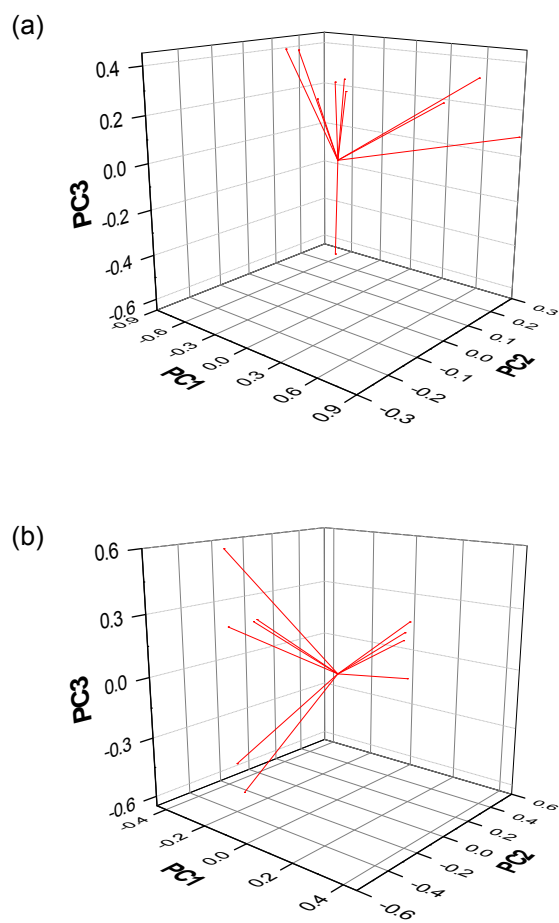


Figure S4. 3D PCA component loading plots of the variables: (a) static cell and (b) flow cell.

7. Reproducibility in Response

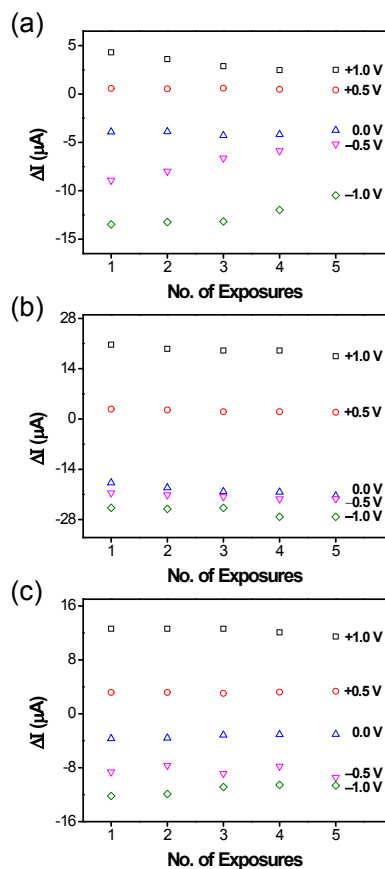


Figure S5. Response extents of PPCL papers recorded upon cyclic exposures to metal ions: a) 100 μM Hg(II), b) 50 μM Ag(I), and c) 100 μM Cr(III).

PPCL papers exhibited good reproducibility in response. PPCL paper-based sensors had prominent responses to Hg(II), Ag(I), and Cr(III). Therefore, the PPCL papers were periodically exposed to the three metal ions. Figure S5 plots the response magnitude of PPCL papers measured upon cyclic exposure of the metal ions. The responses to Ag(I) and Cr(III) were quite reproducible while the responses to Hg(II) became gradually reduced in extent (Table S3). There were particularly some variations in response at relatively high potentials such as -1.0 and $+1.0$ V. The reactive sites of PPCL papers would be saturated under the repeated exposures, probably leading to decrease in reproducibility. To improve the reproducibility in

response, thus, we electrochemically reset the PPCL paper electrode by applying a counter potential before re-exposure. Figure S6 gives information on the electrochemical reset process of the sensing system. Fortunately, PPCL papers showed much improved reproducibility in response, as seen in Figure S7. The cyclic tests could be carried out more than five times without significant deviation (relative standard deviation: 2.8 to 6.5%) in response.

Table S3. Reproducibility of current change values measured in Figure R1: averages and standard deviation (SD) of five runs are given.

Potential (V)	Hg(II)		Ag(I)		Cr(III)	
	ΔI (μA)	SD	ΔI (μA)	SD	ΔI (μA)	SD
+1.0	3.15	0.79	19.15	1.16	12.27	0.51
+0.5	0.52	0.07	2.24	0.38	3.18	0.12
0.0	-4.00	0.22	-19.75	1.37	-3.31	0.31
-0.5	-6.92	1.53	-21.56	0.71	-8.48	0.75
-1.0	-12.47	1.25	-25.80	1.32	-11.23	0.77

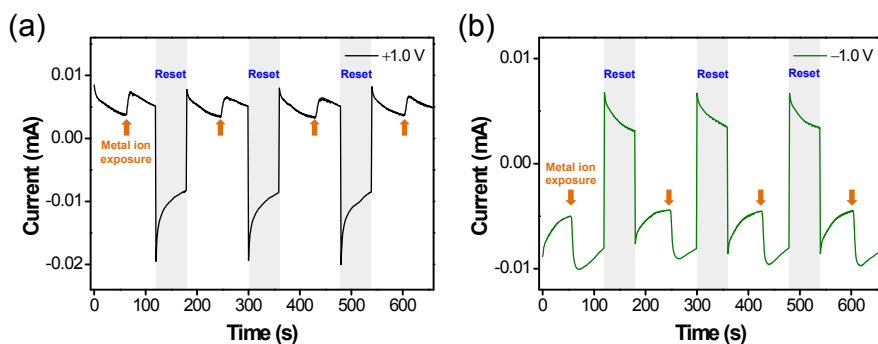


Figure S6. Response profiles showing the electrochemical reset process of PPCL paper electrodes when cyclic exposed to 100 μM Hg(II), in which the reset period was gray-colored.

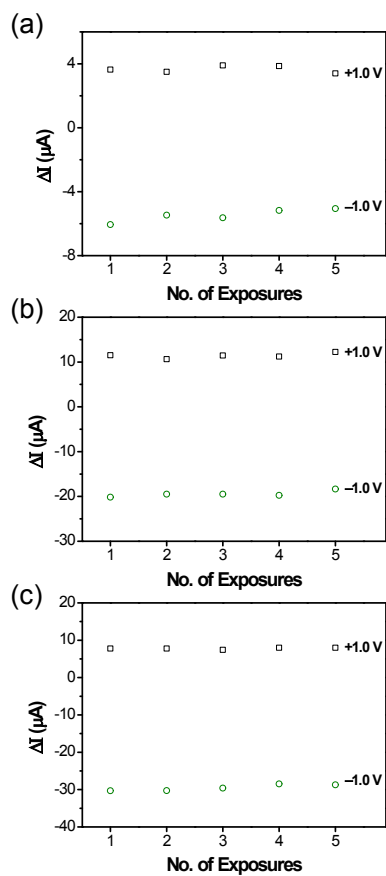


Figure S7. Response extents of PPCL papers recorded upon cyclic exposures to metal ions, where the PPCL paper electrode was reset by applying a counter potential after metal ion exposure: a) 100 μM Hg(II), b) 50 μM Ag(I), and c) 100 μM Cr(III).

8. Kinetic Binding Parameters

Table S4. Kinetic parameters obtained from the kinetic model of polypyrrole-metal ion binding on the PPCL paper surface.

Metal ions	Potential (V)	K_{eq} ($10^{-2} M^{-1}$)	k_f ($10^{-3} s^{-1}$)
Hg(II)	+1	53.9	13.2
	0	50.1	6.8
	-1	66.7	9.5
Ag(I)	+1	16.6	32.6
	0	15.5	12.9
	-1	18.6	5.3
Pb(II)	+1	11.0	3.6
Ni(II)	+1	11.3	3.3
Cd(II)	+1	10.9	17.8
	-1	10.9	8.8
Cr(III)	+1	10.9	10.3
	0	11.4	2.3
	-1	11.5	1.5

9. Real Sample Test

Our study aims ultimately to develop a rapid detection system of heavy metal contamination in water for living. Tap water is usually safe, whereas groundwater can be abruptly contaminated by unexpected events. Thus, a concerned target could be groundwater that is one of the important water sources. People are widely using groundwater for drinking, farming, and so on. It is known that more than 50% of the US population depends on groundwater for drinking water. Therefore, in this work, we used a groundwater sample for the real sample analysis. The groundwater sample, known to be unfit for drinking, was collected from a site in Gwangju, South Korea. We assumed that the groundwater was contaminated with the three metal ions, Hg(II), Ag(I), and Cr(III). The composition of the groundwater, except the three metal ions, are presented in Table S5. Sodium, calcium, and silicon were contained in the real sample at high portions of 960, 670, and 730 μM , and smaller amounts of magnesium and sulfur were observed.

Table S5. Major components of the real sample (groundwater, pH 7.2) used.

Components	Conc. (μM)
Na	960
Mg	120
Ca	670
S	69
Si	730

We first examined whether the selectivity of PPCL papers in response is still maintained in the real sample. The real-time responses of the PPCL papers to the metal ions in the real sample were measured using the flow cell and are presented in Figure S8. It appears that the overall responses of PPCL in the real sample were more intensive than those in the standard sample prepared in the laboratory. The PCA scores

of the data set are plotted in Figure S9. Fortunately, the selectivity of PPCL papers toward the three metal ions was reasonably maintained although there were some discrepancy in the data position, as shown in Figure S9a. In PC1–PC2 plane which accounts for 88.5% of the data variance (Figure S9b), metal ion data detected in the real sample are found to be positioned in the data region of the same metal ions collected from the standard solution.

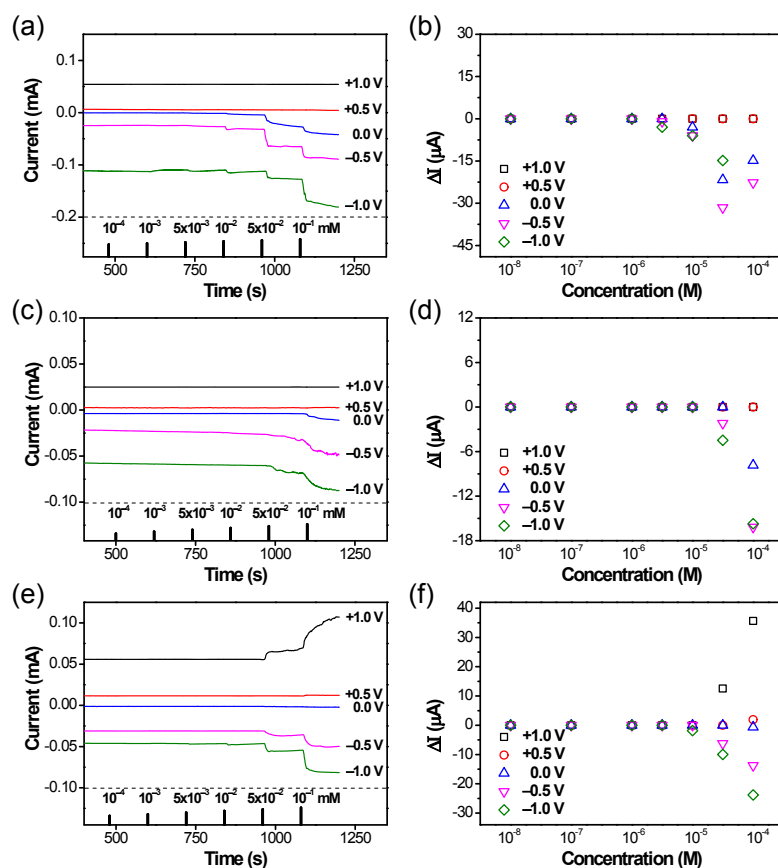


Figure S8. Real-time responses of the PPCL papers in the flow cell measured at different applied potentials: a) Hg(II), b) Ag(I), and c) Cr(III) in the real sample.

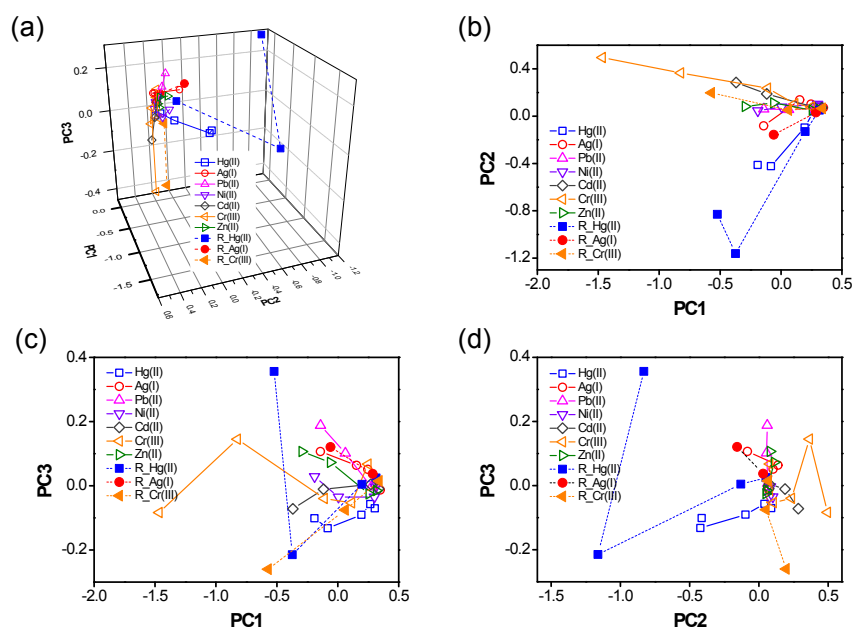


Figure S9. PCA plots of the responses of PPCL papers calculated using the data from Figure S10, in which the score points from the same metal ions were connected by a solid line (the existing data set) or dotted line (the real sample) in the order of concentration: (a) 3D plot, (b) PC1–PC2 plane, (c) PC1–PC3 plane, and (d) PC2–PC3 plane.

In both PC1–PC2 and PC2–PC3 plots, particularly, an easy discrimination of Hg(II) was still possible because the data scores for Hg(II) were clustered in the region that are completely separated from the others. The difference between the real/standard samples in response would be the presence of interfering ions. Nevertheless, PPCL papers had excellent selectivity toward Hg(II), which is likely due to their superior absorption capability for Hg(II). The ICP analysis gave the information that the absorption of Hg(II) by PPCL papers in the real sample was 93–97%, which was slightly higher than that in the standard sample over the same period.